COBEM 2021 26th International Congress of Mechanical Engineering
November 22-26, 2021, Virtual Congress, Brazil

COB-2021-2132

A MAGNETOCALORIC ROTARY REFRIGERATOR PROCESSES SIMULATOR USING A STEPWISE MODELLING APPROACH

Victória Heringer Saippa
Julio Cesar Guimarães Tedesco
Leôncio Diógenes Tavares Câmara
Polytechnique Institute of Rio de Janeiro State University (IPRJ/UERJ), Rua Bonfim 25, Vila Amélia, Nova Friburgo - RJ, CEP 28625-570, Brazil.
vicheringersaippa@gmail.com, tedesco.jcg@gmail.com, diogenescamara@gmail.com.

Abstract. *Magnetic refrigeration has been considered a promising technology. Based on the magnetocaloric effect, one of its great advantages is that it offers an overall lower environmental impact compared to conventional refrigeration. In addition to its modeling simulations of thermodynamic processes, it can provide important information in the development and optimization of experimental devices. A complete process simulator for a rotary cooler was executed in order to study the performance of the processes under different conditions. A step-by-step modeling approach was applied, simplifying the heat transfer phenomena. Certain magnetocaloric materials were chosen as the refrigerant material because of their magnetic transition near to room temperature: Gadolinium metal, $Gd_5Ge_2Si_2$ ternary compound, a $La(Fe\text{-}Mn\text{-}Si)_{13}$-H compound, and a Ni-Co-Mn-In Heusler alloy. The system assumes a clockwise rotating magnetic material wheel with a closed counterclockwise water flow loop, through which percolates the six porous areas of the magnetocaloric material, and hot/cold heat exchangers. The simulator was able to represent both the transient aspects and the conditions of the steady-state of the processes, considering the temporal performance and numerical stability. The inversion of heat transfer profiles throughout the process was used as the limit in calculating the maximum heat transfer absorption in the cold exchanger.*

Keywords: *magnetic refrigeration, magnetocaloric effect, rotary refrigerator, stepwise modelling, transient magnetic regenerative process.*

1. INTRODUCTION

Society has been increasingly concerned with the environment. The research for technological solutions that generate less impact on climate change has been progressively becoming a priority throughout the world. The environmental impact of CFCs and HCFCs refrigerant gases is well known and since 1989 the production and use are restricted (Beshr *et al.*, 2016 and Benhadid-Dib and Benzaoui, 2012). Therefore, new projects and alternatives have been developed on refrigerant fluids and their products, devices, manufacturing processes, and maintenance procedures. Nevertheless, one of the eco-friendlier solutions for this issue may lie within the technology of magnetic refrigeration.

Magnetic cooling is based on the magnetocaloric effect (MCE), which is the thermal response when a material is subjected to a magnetic field variation. Discovered in the 19th century (Smith, 2013), MCE was first used in cryocooling applications around the mid 20th century. Since then many investigations were conducted to study the performance of magnetic refrigeration (Tishin and Spichkin, 2003 and Yu *et al*., 2010). However, it is only from 1997, when Pecharsky and Gschneidner discovered the giant magnetocaloric effect (GMCE), that part of the scientific community began a search for materials and methods aimed at the large-scale commercial application of magnetic refrigeration (Pecharsky and Gschneidner, 1999 and Tishin and Spichkin, 2014). Certain challenges remain: the materials most suitable for this application must have magnetic transitions at temperatures close to the environment; and the need for relatively high magnetic fields. In the late 1970s, a magnetic refrigerator operating at room temperature was built using Gadolinium metal (Gd) as a refrigerating element. However, it is also important to notice the high cost of this technology, so its optimization is extremely important (Ross Jr, 2002 and Tura, and Rowe, 2014). In 2015, a wine chiller prototype was unveiled at the Consumer Electronics Show in Las Vegas, US. The wine cooler is designed to reach a temperature of 8°C to 12°C in an average room temperature environment. Another recent and very interesting and complete work has been developed by Trevizoli *et al.* (2016a) and Trevizoli *et al.* (2016b). Some older studies projected an efficiency around 20% to 30% higher in refrigerators based on MCE compared to conventional ones, which operate in vapor compression systems (Yu *et al*., 2010). However, experimentally, these predictions may not be as advantageous (Steven Brown and Domanski, 2014). Despite this, the technology may still evolve. Furthermore, cooling systems based on magnetocaloric materials will operate with less noise due to the absence of a compressor. This

technology makes use of solid materials as coolants instead of gaseous refrigerants, and a water-based mixture is used to promote the heat exchange, which is more environmentally friendly (Cooling Post, 2015).

Besides taking a long time, the construction of prototypes can be expensive. Therefore, simulations of the several physical processes and phenomena present in the operation of these devices, followed by the necessary analysis, can be useful in providing information and tools to predict and solve possible problems and increase the efficiency of the device (Tušek *et al*., 2010 and Tura and Rowe, 2014). In this sense, simulations of the thermodynamic processes, beyond their modeling, can provide important information in the development and optimization of the experimental devices (Huang *et al*., 2019).

There are many designs for these systems. One of these is the rotary refrigerators, which presents several challenges in terms of complexity when comparing to reciprocating ones. However, these challenges are compensated by several of its properties (Vuarnoz *et al*., 2011).

In this work, a full process simulator, able to assess the thermal response and mapping some thermal properties of magnetocaloric refrigerator processes, was implemented to study the processes' performance over different conditions. A stepwise modeling approach was applied, simplifying the phenomena of heat transfers. It is worth highlighting a feature of the simulator under development. Obtaining detailed and complete results of the fluid temperature behavior in numerical modeling requires knowing all the various physical properties of materials and characteristics of the parts of the system. This need implies performing heavy and complex computational modeling. However, the proposed approach in this project allows to simplify the process and reduce processing time. Another adopted simplification concerns the thermal capacity of the materials. It is known that the thermal capacities of magnetic materials can vary considerably around T_C. However, as one of the goals of this project is to evaluate the limits and responses of the simulator described in this text, the thermal capacities were considered constant. Certain magnetocaloric materials were chosen as refrigerant materials. Among these materials are Gd metal, $Gd_5Ge_2Si_2$ ternary compound, La(Fe-Mn-Si)$_{13}$-H compound, and Ni-Co-Mn-In Heusler alloy, which present magnetic transition near to room temperature. The routine considers a rotating clockwise magnetic material wheel with a counterclockwise closed flow loop of water, through which percolates the six porous areas of the magnetocaloric material, and hot/cold heat exchangers. The simulator was able to represent the transient aspects as well as the steady-state conditions of the processes, considering both: time performance and numerical stability. The inversion in heat transfer profiles along the process was used as a limit in the calculation of the maximum heat transfer absorption in the cold exchanger (Câmara and Tedesco, 2021).

2. DESCRIBING THE ROTARY DESIGN AND COMPUTATIONAL APPROACH

When the temperature of a material changes significantly due to a change in the applied magnetic field, this material is said to have a magnetocaloric effect. In order to measure the MCE, two physical quantities are used: the adiabatic variation of temperature, ΔT, and the isothermal variation of entropy, ΔS. These variations are called magnetocaloric potentials and they quantify the magnetocaloric effect. Using Maxwell relations, it is possible to obtain expressions of these two potentials from magnetization and specific heat data as a function of both temperature and applied magnetic field. It is worth noting that the temperature variation ΔT, although it can be measured directly, its somewhat difficult to obtain through physical experiments when small samples are studied (Tishin and Spichkin, 2003). The magnetocaloric potentials are:

$$\Delta S(T) = \int_{B_i}^{B_f} \frac{\partial M(B,T)}{\partial T} dB \tag{1}$$

and,

$$\Delta T(T) = -\int_{B_i}^{B_f} \frac{T}{C_p(B,T)} \frac{\partial M(B,T)}{\partial T} dB \tag{2}$$

It is worth noting that both potentials depend on the temperature and the variation of the applied magnetic field, i.e. $\Delta B = \left(B_f - B_i\right)$. In any case, the curves $(-\Delta S)\ vs.\ T$ and $\Delta T\ vs. T$ have similar shapes and have a maximum when the derivative of $M(B,T)$ in terms of T is maximum. This is why researchers are looking for new materials which have a magnetic transition close to room temperature (Tishin and Spichkin, 2003).

The operation of a refrigerator based on the magnetocaloric effect depends on the increase in temperature T due to the ΔB field variation (Tishin and Spichkin, 2003). Thus, to run the simulator developed in this work, the value of this increment of T as an input is needed. Here we have, the curves of $\Delta T\ vs. T$ for a given ΔB (Kitanovski *et al*., 2015). To compare how the response of the simulator depends on the used magnetic material, four different materials were chosen. All of these materials present magnetic transition T_C close to room temperature: Gd metal (usual material in magnetic refrigeration); the $Gd_5Ge_2Si_2$ ternary compound (famous alloy responsible for the study of the giant magnetocaloric effect); La(Fe-Mn-Si)$_{13}$-H compound with Mn concentration equal 0.30 (its nominal composition is $LaFe_{11.41}Mn_{0.30}Si_{1.29}H_{1.65}$); and Ni-Co-Mn-In Heusler alloy (nominally as $Ni_{45.3}Co_{5.1}Mn_{36.1}In_{13.5}$). As indicated, these materials are interesting in the study of MCE for specific reasons, whether due to the magnitude of the effect or the

historical importance of the material in the area. For commercial applications, the ΔB field variation should not be too high, or at least it should be achieved by permanent magnets. However, there are not enough experimental data to compare the behaviors of these materials due to a low ΔB. Thus, the value of the magnetic flux variation $\Delta B = 1.5\,T$ was chosen. In order to input the thermal response of the above-mentioned materials due to $\Delta B = 1.5\,T$ in the simulator, the related $\Delta T\ vs.\ T$ curves were fitted using an expression that is composed by exponential and lorentzian functions. Then, it was possible to obtain the values of the temperature increments used in the simulation for each material at each studied temperature. The result of these considerations can be seen in Figure 1. By this process, it was possible to introduce the magnetocaloric effect in the simulator.

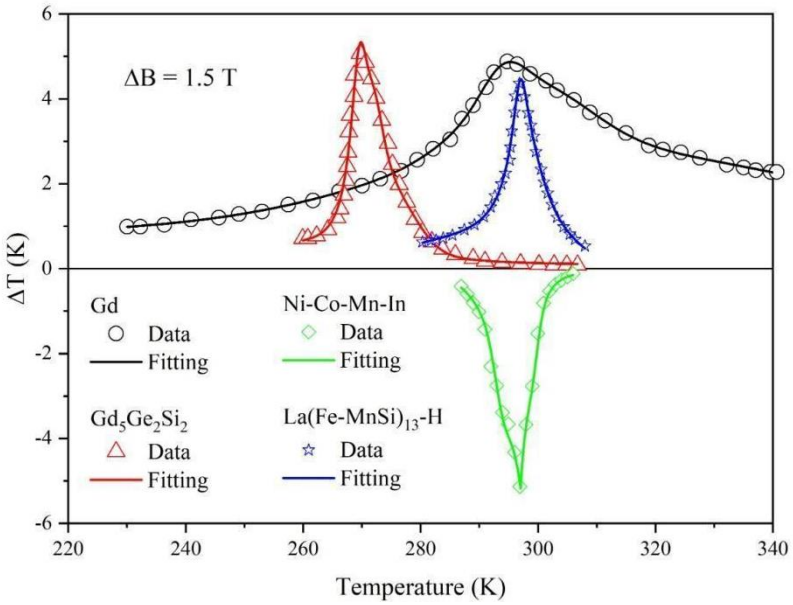

Figure 1. The $\Delta T\ vs.\ T$ data and fittings curves for Gd metal, $Gd_5Ge_2Si_2$ and La(Fe-Mn-Si)$_{13}$-H and Ni-Co-Mn-In compounds due to $\Delta B = 1.5\,T$. The open symbols represent the temperature changing ΔT and the lines are the fittings using exponential and lorentzian functions.

In Figure 1 it is possible to compare the different shapes and amplitudes of the curves from the different compounds chosen. These differences directly influence the response of the simulator. The peak of the ΔT curve of Gd is around 295 K and its amplitude is closed to 4 K. The width of this curve is larger than the others. Because of its amplitude and curve shape, Gd is a well-regarded material for magnetic refrigeration applications. The thermal response of $Gd_5Ge_2Si_2$ compound is narrower and shifted to lower temperatures than Gd metal. Its maximal variation is close to 5K and it is around 270 K (Sigma-Aldrich, no date). The La(Fe-Mn-Si)$_{13}$-H compound presents its response due to $\Delta B = 1.5\,T$ as shown in Figure 1, such as the other materials. The peak of this curve is about 297 K and its amplitude is 4 K, approximately, and the shape of it is similar to $Gd_5Ge_2Si_2$ compound thermal response curve (Basso *et al.*, 2015). Finally, the Ni-Co-Mn-In Heusler alloy presents the inverse magnetocaloric effect. It means that the material cools with the application of a magnetic field. The shape of the curve for this material is similar to $Gd_5Ge_2Si_2$ and La(Fe-Mn-Si)$_{13}$-H compounds. Its peak is also around 297 K and its amplitude is close to -5 K. As the Heusler alloy presents a negative peak, the obtained expression from the fitting was multiplied by (-1) in order to compare the different behaviors of the materials (Chen *et al.*, 2016, and Puglielli et al., 2020). For a complete analysis of this material, the thermomagnetic scheme should be changed, including inverting the thermal reservoir's positions.

The most commonly used thermomagnetic closed cycle for this kind of system is the Brayton. It is composed of four thermodynamic processes, creating the closed cycle shown in Figure 2 below. The Brayton cycle consists of two isentropic processes, $E_1 \rightarrow E_2$ and $E_3 \rightarrow E_4$, and two isofield processes, $E_2 \rightarrow E_3$ and $E_4 \rightarrow E_1$.

As indicated in Figure 2, the entropy S of a magnetocaloric material depends on the temperature T and the field B. Then, it is important to know the entropy $S_0(T)$ with no applied magnetic field and the entropy $S_B(T)$ with $B \neq 0$. In this case, the functions were inverted. Starting at point E_1, a magnetic field B is applied. Then, adiabatically, the system reaches the state E_2: the magnetocaloric material has its temperature raised while its entropy is kept constant. At the point E_2, a fluid is used to reduce the temperature of the material while the field B is still applied. Once at the state E_3, the magnetic field B is taken away and the temperature of the material decreases up to point E_4 performing an isentropic process ($S = constant$). Finally, from state E_4 to state E_1, the field is kept null, and a fluid provides heat to the regeneration material from the cold source.

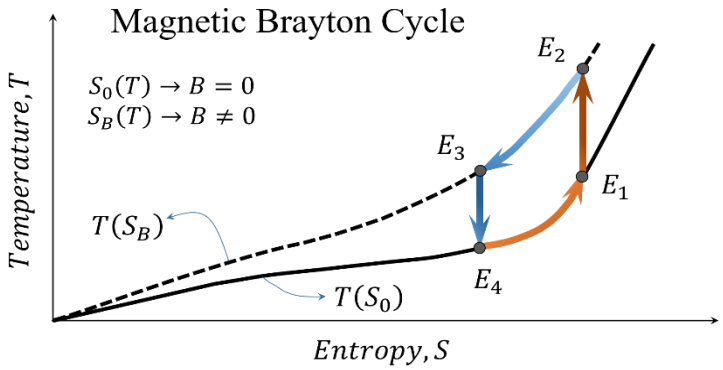

Figure 2. The thermomagnetic Brayton closed cycle used in the simulation. The processes $E_1 \rightarrow E_2$ and $E_3 \rightarrow E_4$ are isentropic, and $E_2 \rightarrow E_3$ and $E_4 \rightarrow E_1$ are isofield processes.

In a refrigerator using a rotary design, two or more sectors composed of magnetic materials can be used to form a wheel to optimize these processes, which can happen simultaneously. In this work, it was chosen a wheel containing six sectors of magnetocaloric material. Assuming water as a heat exchanger, the flow diagram can be seen in Figure 3.

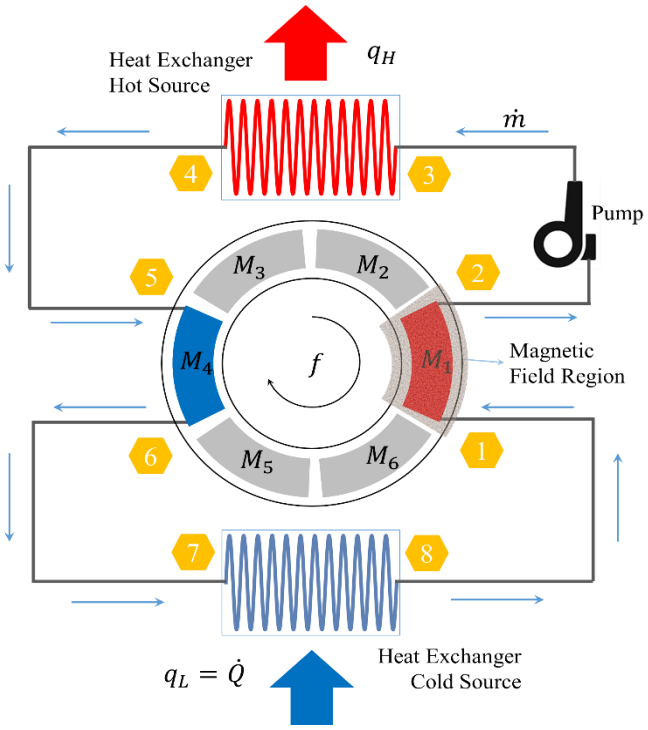

Figure 3. The water flow diagram showing the heat exchangers (hot source and cold source) and the synchronized regenerator numbered sectors. A pump generates the flow, that passing through the system, percolating the regenerator material sectors. The magnetized section is the shadow region as shown. The numbers in the hexagons indicate the entries and the exits in each stage of the process.

In Figure 3, the fluid flow scheme is divided into eight points. The sectors of the regenerator material are numbered from 1 to 6. Sectors n and n+3 will be synchronized, as sector 1(M_1) and sector 4 (M_4), as shown. Magnets provide $B = 1.5\,T$ in the indicated region. When the material in the sector M_1 enters in the magnetic field region (process $E_1 \rightarrow E_2$), the fluid enters in point 1 and leaves at point 2 percolating the regenerate material, exchanging heat with this sector and performing the $E_2 \rightarrow E_3$ isofield process. Concomitantly, sector M_4 in the region without the magnet field (process $E_3 \rightarrow E_4$), receives the flow in point 5 and leaves at point 6 after exchanging heat (process $E_4 \rightarrow E_1$). When the sectors are entering and leaving from the magnetic field region, the adiabatic processes occur. The pump, operating between points 2 and 3, provides the water flow rate ($\dot{m}$) through the mechanism. Furthermore, the flow exchanges heat with the hot and cold sources with rates q_H and q_L, respectively, located between points 3 and 4, and 7 and 8. As indicated, the wheel of regenerate material sectors operate clockwise in a frequency f and the heat exchanger fluid flows counterclockwise.

Studies on the distribution of permanent magnets and electromagnets to optimize magnetic field lines have already been carried out, however only a few prototypes with permanent magnets are proposed (Gschneidner and Pecharsky, 2008, and Yu *et al*., 2010, Bjørk et al., 2010). Several projects intended to simulate and test these distributions to obtain both: high intensity and uniformity of the magnetic field (Bjørk *et al*., 2010). As indicated, many prototypes have already been built. Electromagnets have the advantage of better handling, however they tend to be expensive and more complicated for home use (Tušek *et al*., 2010, and Vuarnoz *et al*., 2011). On the other hand, obtaining an optimized field line configurations with permanent magnets becomes unfeasible. To help with this problem, many researchers use the finite element method as a tool to simulate magnetic field lines (Kitanovski *et al*., 2015). However, the supply of the magnetic field is outside the scope of this work, it was only postulated, as shown in Figure 3.

The fluid temperatures throughout the entire system were calculated using determined techniques. Some softwares can calculate the desired physical properties in similar systems. These softwares usually solve the partial differential heat equations that can express the MCE. In fact, the results obtained by solving these equations are rich, however they present a high computational cost. In addition, they do not provide simple solutions. A simpler way to deal with this problem is to assume the energy balance in the heat exchange of the thermodynamic system (Vuarnoz *et al*., 2011, and Albertini *et al*., 2017). Thus, the transient modeling approach for fluid temperature corresponds to:

$$\rho_f c_{pf} V_f \frac{dT_f}{dt} = \dot{m}\, c_{pf}\left(T_{fin} - T_{fo}\right) + h_n A_n \left(T_n - T_{fo}\right) \tag{3}$$

The solution of equation 1 describes the fluid temperature, T_f, in heat exchangers, i.e., hot and cold sources, and the pore spaces of the magnetocaloric materials. The physical quantities of the fluid were expressed in terms of ρ_f, c_{pf}, V_f, and represent density, heat capacity and volume, respectively. Besides, $\dot{m}$ is the mass flow rate. T_{fin} is the entrance temperature of the fluid in the heat exchangers, while T_{fo} is the exit temperature. They are related to the heat flows q_H and q_L. In addition, h_n is the advection coefficient, A_n is the heat transfer area, and, T_s represents the temperature of the heat exchanger. The n-sub index is related to the hot/cold source, denoted by subindex 'e', and the regenerator material, when sub index 's' is adopted. The energy transient term results from the contribution of the energy transport along the borders plus the advection. In this model, it is considered an ideal uniform value of temperature along the fluid volume system in which the temperature at the exit is the same as the temperature in the interior of the system.

For the materials energy balance model, the transient term is the contribution of the advection heat transfer, as follows:

$$\rho_s c_{ps} V_s \frac{dT_s}{dt} = -h_s A_s \left(T_s - T_{fo}\right) \tag{4}$$

As indicated above, the subscript utilized in the equation (2) refers to solid material, i.e. c_{ps}, ρ_s and V_s which represent respectively the heat capacity, density of material and volume of the material bulk sector. Finally, h_s and A_s are the advection coefficient and the heat transfer area of the bulk material, respectively, while T_{fo} is the fluid temperature after leaving the magnetocaloric pores.

It was considered the same bulk sector volume for all the four materials. Some assumptions were made for the model: no energy loss along the pipes and constant heat rate in the cold source of the heat exchanger. Furthermore, it is important to note that the advection coefficients provides the simplicity of this model. Various physical properties of materials and characteristics of the system parts are required to produce a complete and reliable numerical modeling of the fluid temperature behavior. This need implies a high computational cost. However, these advection coefficients simplify the process and greatly reduce the processing time. Another simplification used concern the thermal capacity of the materials. The thermal capacities of magnetic materials tend to vary widely around T_C, with or without the application of a magnetic field. However, as one of the objectives of this project is to evaluate the limits and responses of the simulator, these thermal capacities were considered constant, i.e. they do not depend either on temperature or on the magnetic field.

The temperatures of the fluid along the path (Figure 3) are labeled as T_1 to T_8 and are related to the points 1 to 8. With the aforementioned considerations, the temperature at point 4 is equal to point 5, $T_4 = T_5$, as well as $T_6 = T_7$, $T_8 = T_1$. Since the pump was considered ideal, $T_2 = T_3$. The stepwise hypothesis means that the magnetized section allows the complete magnetization of the regenerate material areas as it moves in the clockwise direction, i.e., there is no partial magnetization of the material pores.

As mentioned previously, the temperature variation (Figure 1) was incorporated in the simulator using the difference ΔT, due to the insertion or removal of the magnetic field, depending on the material. The steps of magnetization and demagnetization are, respectively:

$$T_s^{i+1} = T_s^i \pm \Delta T \tag{5}$$

In equation (3), the plus sign is used for the application of a magnetic field and the minus sign for its removal. The inversion in the heat transfer profiles along the process was used as a limit in the calculation of the maximum heat transfer absorption in the cold exchanger. The inversion takes place when the process ceases to operate as a refrigerator, i.e. when the cold source does not have a satisfactory temperature gradient to heat absorption. For the demagnetization cases (sector M_4), it was used the the previously mentioned magnetization equations but with the opposite sign (sector M_1).

3. RESULTS AND DISCUSSION

Some physical parameters were assumed in order to input these values on the simulator (Table 1). The volume values (V_f and V_s) were chosen based on a project for a magnetic refrigerator being developed at the IPRJ/UERJ (Câmara and Tedesco, 2021). The same for the area quantities (A_e for cold/heat exchangers and A_s for magnetocaloric material). Based on the average values in the literature for water, Gd and common cold and hot exchangers, advection coefficients h_e (for cold/heat sources) and h_s (for solid coolant) each value was assumed. As said before, the heat capacity and density values were considered as an average at the transition temperature, around room temperature, except for the $Gd_5Ge_2Si_2$, for which the values of density and heat capacity were used at $T = 270\ K$ (Palacios *et al.*, 2010). The time step considered in the simulator was $10^{-3}\ s$.

Table 1. The values of input parameters for the simulations performed measured at 298 K.

Physical Quantities	Values
ρ_f	$1000\ kg \cdot m^{-3}$
c_{pf}	$4186\ J \cdot kg^{-1} \cdot K^{-1}$
V_f	$3 \cdot 10^{-5}\ m^3$
h_e	$2000\ W \cdot m^{-2} \cdot K^{-1}$
A_e	$0.88\ m^2$
V_s	$2.275\ \times 10^{-5}\ m^3$
h_s	$1000\ W \cdot m^{-2} \cdot K^{-1}$
A_s	$0.22\ m^2$
Gd *	
ρ_s	$7630\ kg \cdot m^{-3}$
c_{ps}	$235.5\ J \cdot kg^{-1} \cdot K^{-1}$
$Gd_5Ge_2Si_2$ **	
ρ_s	$5700\ kg \cdot m^{-3}$
c_{ps}	$420\ J \cdot kg^{-1} \cdot K^{-1}$
$La(Fe\text{-}Mn\text{-}Si)_{13}$-H †	
ρ_s	$7245\ kg \cdot m^{-3}$
c_{ps}	$460\ J \cdot kg^{-1} \cdot K^{-1}$
Ni-Co-Mn-In ◊	
ρ_s	$8000\ kg \cdot m^{-3}$
c_{ps}	$350\ J \cdot kg^{-1} \cdot K^{-1}$

* (Dan'kov *et al*., 1998);
** (Palacios *et al.*, 2010, and AMERICAN ELEMENTS site, no date);
† (Basso *et al.*, 2015, and Li *et al*., 2019);
◊ (Chen *et al*., 2016, and Puglielli *et al*., 2020).

The simulator allows a large number of analyses and enables changing several parameters. For this work, in order to analyze the influences of the materials and their different behaviors, the physical parameters listed in the Table 1 were chosen. One of the parameters used in this study is an induced power at the cold source ($q_L = \dot{Q}$). The simulations demonstrated that for each peak profile of magnetization, $\Delta T\ vs.T$, the simulator induces a different regime in the process, thus it varied the mass rate, $\dot{m}$, power, Q, and rotation frequency f.

The following figures are showing the flow temperature behavior of T_2, T_4, T_6, T_8, i.e., in points 2, 4, 6, 8 in function of time. In this work, for the refrigerator condition, the temperature at the point 6, T_6, before the cold source, has to be lower than the temperature at the point 4, T_4. Furthermore, the temperature at point 2 (T_2) has to be higher than the temperature at point 8 (T_8) after the cold source.

In Figure 4 it is possible to see the response of flow temperatures for the regenerator material gadolinium with the initial condition of temperature at $293.15\ K$, power of $\dot{Q} = 200\ W$, mass flow rate of $\dot{m} = 20 \times 10^{-3} kg\ s^{-1}$ and

frequency of 1 Hz. The metal of Gd presented a large peak as seen in Figure 1. For this result, a variety of values of these parameters were tested in order to discover the best conditions for this refrigeration regime, and to analyze the sensitivity of the simulator. For the same power and mass flow rate, but a lower frequency, the simulator still responds as a refrigerator, although the variation of T_6 was smaller than the presented at Figure 4. Only changing the value of mass flow rate $\dot{m}$ to an higher one, the variation of T_6 was also lower than the following figure. On the other hand, a higher frequency changed completely the disposition of temperature, all the temperatures were lower than T_4, as if a large amount of heat has been removed from system. The opposite happened at a higher power, all the temperatures were higher than T_4, changing the behavior from a refrigerator to a heat pump-like system.

The Figure 5 shows the flow temperature along the process position in the stead state, using initial condition of temperature at 270 K, power of $\dot{Q} = 100\ W$, mass flow rate of $\dot{m} = 35 \times 10^{-3} kg\ s^{-1}$, frequency of 0.1 Hz and $Gd_5Ge_2Si_2$ as magnetocaloric material. Comparing with previous results, this compound needed a lower temperature, power and frequency but a higher mass flow rate to achieve the refrigerator regime. The temperature T_6 reached values very close to T_4, approximately $|T_6 - T_4| = 0.15\ K$, while for the system using Gd reached $|T_6 - T_4| \sim 1.6\ K$. The $Gd_5Ge_2Si_2$ presents a shifted peak, around 270 K, and for this reason, the response of the system at a room temperature was a heat pump-like system. For lower power and mass flow rate, the flow temperatures kept a refrigerator regime, but the configuration of Figure 4 presented a better stability. A higher power was tested, but the decrease of cold source temperature happened just in the initial moments and returned to the initial temperature.

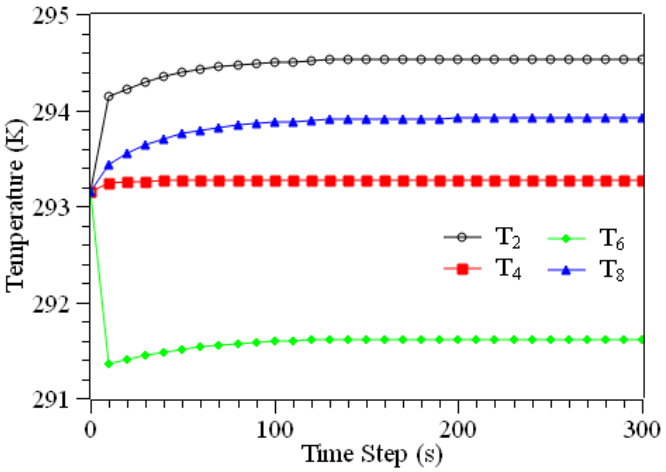

Figure 4. The simulations of T_2, T_4, T_6 and T_8 and how they develop in function of time for Gd metal. The parameters are $T_i = 293.15\ K$, $\dot{Q} = 200\ W$, $\dot{m} = 20 \times 10^{-3} kg\ s^{-1}$ and $f = 1\ Hz$.

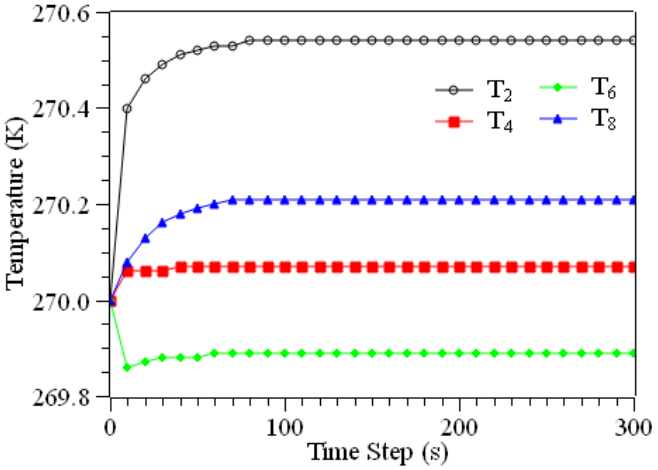

Figure 5. The simulations of T_2, T_4, T_6 and T_8 and how they develop in function of time for $Gd_5Ge_2Si_2$ compound. The parameters are $T_i = 270\ K$, $\dot{Q} = 100\ W$, $\dot{m} = 35 \times 10^{-3} kg\ s^{-1}$ and $f = 0.1\ Hz$.

Changing the material for the La(Fe-Mn-Si)$_{13}$-H compound and using the initial temperature $T_i = 293.15\,K$, the parameters that provided a refrigerator regime are $\dot{Q} = 200\,W$, $\dot{m} = 20 \times 10^{-3} kg\,s^{-1}$ and $f = 1\,Hz$, the same used with Gd metal. The flow temperatures are shown in Figure 6. This response was similar to Figure 4, despite the fact the compound has a lower cold source temperature in the steady-state. It is also important to notice that the peaks of the two materials are near, but the Gd metal presents the higher and larger width.

The Ni-Co-Mn-In Heusler alloy is used to provide the fluid temperature in the Figure 7 using $T_i = 293.15\,K$. The parameters used in this case are $\dot{Q} = 100\,W$, $\dot{m} = 100 \times 10^{-3} kg\,s^{-1}$ and $f = 0.1\,Hz$. As showed in Figure 1, this alloy presents a negative peak. For this reason, a negative sign multiplying the $\Delta T\,vs.T$ curve was used, to obtain the cold configuration. In spite of this fact, the Heusler alloy has a similar peak to the La(Fe-Mn-Si)$_{13}$-H compound. In terms of flow temperature, this alloy does not have good cooling capacity. For this alloy, in most parts of the configuration, the temperature of the cold source output (T_8) was higher than the temperature at the exit of the magnetization stage.

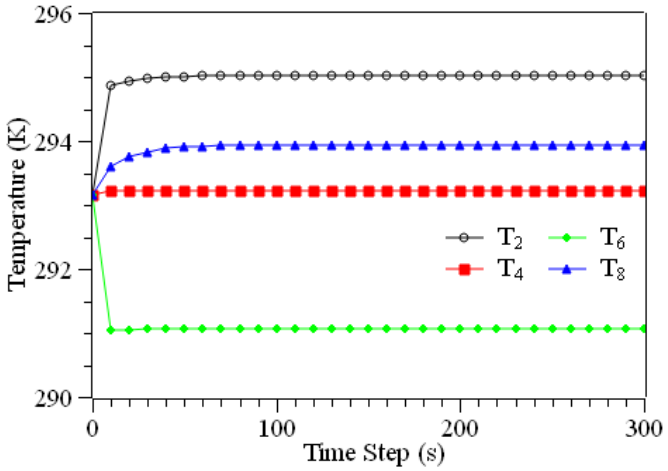

Figure 6. The simulations of T_2, T_4, T_6 and T_8 and how they develop with time for La(Fe-Mn-Si)$_{13}$-H compound. The parameters are $T_i = 293.15\,K$, $\dot{Q} = 200\,W$, $\dot{m} = 20 \times 10^{-3} kg\,s^{-1}$ and $f = 1\,Hz$.

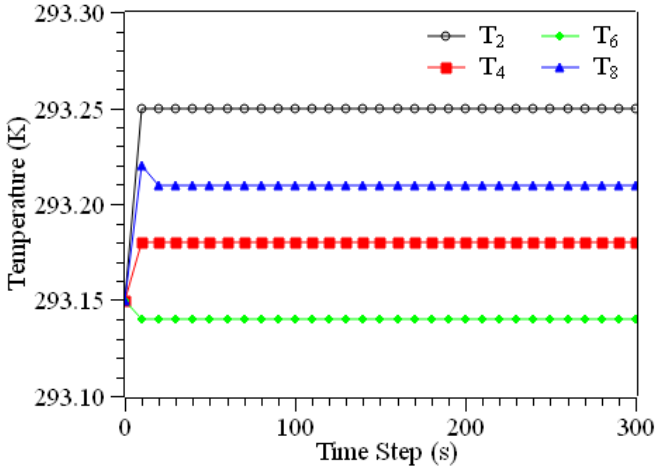

Figure 7. The simulations of T_2, T_4, T_6 and T_8 and how they develop with time for Ni-Co-Mn-In Heusler alloy. The parameters are $T_i = 293.15\,K$, $\dot{Q} = 100\,W$, $\dot{m} = 100 \times 10^{-3} kg\,s^{-1}$and $f = 0.1\,Hz$.

All the results presented showed a good stability. Moreover, they exhibited a sensitive dependency to the curve shapes and amplitudes of $\Delta T\,vs.T$. The entry simulator parameters, T_i $\dot{Q}$, $\dot{m}$ and f are as dependent on the thermal response of the materials, as on the physical properties of the materials.

It is worth noting that some alloys need lower operating frequencies, while it is still unclear why La-alloy presented a larger temperature span than Gd, for the same cooling capacity. In fact, this interesting property is what inspired this work. It is still necessary to explore the limits and the responses of the simulator in order to understand these different behaviors.

4. CONCLUSIONS

This work analyzed the thermal responses of four different materials in a thermomagnetic system, based on a magnetocaloric effect. A rotary design was considered with six areas of magnetocaloric material rotating clockwise with an anticlockwise closed flow loop of water. Moreover, a simpler way of dealing with the temperature prediction problem was developed.

The profile of each material showed a very representative dependency on the curve of thermomagnetic response, $\Delta T \; versus \; T$, and it reflected in the physical parameters needed to guarantee a cooling regime. Even with a simple numerical method, there were no interferences, as shown by a tendency line in the results. It was possible to verify how power, flow rate and frequency affected the scheme. The calculations indicated that the system is very sensitive to the parameters variation.

As one can see, depending on the material, certain simulator inputs are different, such as the operating frequencies and power rating. Furthermore, the compound La (Fe-Mn-Si)$_{13}$-H had a greater temperature amplitude than Gd, since the ΔT of Gd is greater. For now, there is no explanation for this phenomenon. In fact, it is still necessary to explore the simulator's response to identify its limits and patterns. One of the perspectives is to test other materials and properties, before implementing other deeper changes to the algorithm.

Further studies can provide more information about the utility of this simple approach.

5. ACKNOWLEDGEMENTS

The authors would like to thank the Brazilian agencies CNPq and FAPERJ for financial support. This study was financed in part by the Coordenação de Aperfeiçoamento de Pessoal de Nível Superior - Brasil (CAPES) - Finance Code 001.

6. REFERENCES

Albertini, F., Bennati, C., Bianchi, M., Branchini, L., Cugini, F., De Pascale, A., Fabbrici, S., Melino, F., Ottaviano, S., Peretto, A., Rosati, J., and Solzi, M., 2017. “Preliminary Investigation on a Rotary Magnetocaloric Refrigerator Prototype”.Energy Procedia, Vol. 142, pp. 1288–1293.

Basso, V., Küpferling, M., Curcio, C., Bennati, C., Barzca, A., Katter, M., Bratko, M., Lovell, E., Turcaud, J., and Cohen, L.F., 2015. “Specific heat and entropy change at the first order phase transition of La(Fe-Mn-Si)13-H compounds”. Journal of Applied Physics, Vol. 118, p. 053907.

Benhadid-Dib, S., and Benzaoui, A., 2012. “Refrigerants and their Environmental Impact Substitution of Hydro Chlorofluorocarbon HCFC and HFC Hydro Fluorocarbon. Search for an Adequate Refrigerant”. Energy Procedia, Vol. 18, pp. 807–816.

Beshr, M., Aute, V., Abdelaziz, O., Fricke, B., Radermacher, R., 2016. “Potential emission savings from refrigeration and air conditioning systems by using low GWP refrigerants”, The International Journal of Life Cycle Assessment, Vol. 22, No. 5.

Bjørk, R., Bahl, C. R. H., Smith, A., Pryds, N., 2010. “Review and comparison of magnet designs for magnetic refrigeration”, International Journal of Refrigeration, Vol. 33, No. 3, pp. 437–448.

Câmara, L. D. T., and Tedesco, J. C. G., 2021. “Simulator development of a rotary magnetocaloric refrigerator by stepwise regenerator modelling approach”. Journal of Physics: Conference Series, Vol. 1730, p. 012070.

Chen, J.-H., Bruno, N. M., Karaman, I., Huang, Y., Li, J., and Ross, J. H., 2016. “Direct measure of giant magnetocaloric entropy contributions in Ni–Mn–In”. Acta Materialia, Vol. 105, pp. 176–181.

Dan’kov, S. Yu., Tishin, A. M., Pecharsky, V. K., and Gschneidner. K.A., 1998. “Magnetic phase transitions and the magnetothermal properties of gadolinium”. Physical Review B, Vol. 57, No. 6, pp. 3478–3490.

Cooling Post, 2015, Debut for magnetic refrigeration wine cooler, Cooling Post, https://www.coolingpost.com/world-news/debut-for-magnetic-refrigeration-wine-cooler/. Accessed 17 June 2021.

AMERICAN ELEMENTS, no date, Gadolinium Silicon Germanium Alloy | AMERICAN ELEMENTS ® | CAS 189118-23-8, https://www.americanelements.com/gadolinium-silicon-germanium-alloy-189118-23-8; Accessed 18 June 2021.

Gschneidner, K. A., and Pecharsky, V. K., 2008. “Thirty years of near room temperature magnetic cooling: Where we are today and future prospects”. International Journal of Refrigeration, Vol. 31, No. 6, pp. 945–961.

Huang, B., Lai, J. W., Zeng, D. C., Zheng, Z. G., Harrison, B., Oort, A., Dijk, N. H. van, and Brück, E., 2019. “Development of an experimental rotary magnetic refrigerator prototype”. International Journal of Refrigeration, Vol. 104, pp. 42–50.

Kitanovski, A., Tušek, J., Tomc, U., Plaznik, U., Ozbolt, M., and Poredoš, A., 2015. "Magnetocaloric Energy Conversion: From Theory to Applications". Springer International Publishing (Green Energy and Technology).

Li, Y. Q., Wu, Q. C., Shen, F. R., Zhou, H. B., Hu, F. X., Wang, J., Sun, J. R., and Shen, B. G., 2019. "Mechanical and magnetocaloric properties of La(Fe,Mn,Si)13Hδ/Cu plates prepared by Cu-binding prior to hydrogenation". Intermetallics, Vol. 106, pp. 124–129.

Palacios, E., Wang, G., Burriel, R., Provenzano, V., and Shull, R., 2010. "Direct Measurement of the Magnetocaloric Effect in Gd5Si2Ge1.9Ga0.1". Journal of Physics: Conference Series, Vol. 200, p. 092011.

Pecharsky, V. K., and Gschneidner, K.A., 1999. "Magnetocaloric effect and magnetic refrigeration", *Journal of Magnetism and Magnetic Materials*, Vol. 85, p. 13.

Puglielli, F., Mussi, V., Cugini, F., Sarzi Amadè, N., Solzi, M., Fabbrici, S., and Albertini, F., 2020. "Scale-Up of Magnetocaloric NiCoMnIn Heuslers by Powder Metallurgy for Room Temperature Magnetic Refrigeration". Frontiers in Energy Research, Vol. 7.

Ross, R. G. J., 2002. "Cryocoolers 11". Springer US (Cyrocoolers).

Smith, A., 2013. "Who discovered the magnetocaloric effect?". The European Physical Journal H, Vol. 38, No. 4, pp. 507–517.

Sigma-Aldrich, no date. Advanced Materials for Magnetic Cooling. Sigma-Aldrich, https://www.sigmaaldrich.com/BR/pt/technical-documents/technical-article/materials-science-and-engineering/solid-state-synthesis/advanced-materials. Accessed 21 June 2021.

Steven Brown, J., and Domanski, P. A., 2014. "Review of alternative cooling technologies". Applied Thermal Engineering, Vol. 64, No. 1, pp. 252–262.

Tishin, A. M., and Spichkin, Y. I., 2003. "The Magnetocaloric Effect and Its Applications". CRC Press, Boca Raton.

Tishin, A. M., and Spichkin, Y. I., 2014. "Recent progress in magnetocaloric effect: Mechanisms and potential applications". International Journal of Refrigeration, Vol. 37, pp. 223–229.

Trevizoli, P. V., Nakashima, A. T., Peixer, G. F., Barbosa, J. R., 2016a. "Performance evaluation of an active magnetic regenerator for cooling applications – part I: Experimental analysis and thermodynamic performance". International Journal of Refrigeration, Vol. 72, pp. 192–205.

Trevizoli, P. V., Nakashima, A. T. and Barbosa, J. R., 2016b. "Performance evaluation of an active magnetic regenerator for cooling applications – part II: Mathematical modeling and thermal losses", International Journal of Refrigeration, Vol. 72, pp. 206–217.

Tura, A., and Rowe, A., 2014. "Concentric Halbach cylinder magnetic refrigerator cost optimization", International Journal of Refrigeration, Vol. 37, pp. 106–116.

Tušek, J., Samo, Z., Šarlah, A., Prebil, I., and Poredoš, A., 2010. "Development of a rotary magnetic refrigerator". International Journal of Refrigeration, Vol. 33, No. 2, pp. 294–300.

Vuarnoz, D., Kitanovski, A., Gonin, C., Egolf, P. W., and Kawanami, T., 2011. "Modeling and Simulation of the Operation of a Rotary Magnetic Refrigerator". Journal of Thermal Science and Technology, Vol. 6, No. 1, pp. 21–33.

Yu, B., Liu, M., Egolf, P. W., Kitanovski, A., 2010. "A review of magnetic refrigerator and heat pump prototypes built before the year 2010". International Journal of Refrigeration, Vol 33, No. 6, pp. 1029–1060.

7. RESPONSIBILITY NOTICE

The authors are the only responsible for the printed material included in this paper.